Orientational discrete breathers in hydrogen-bonded chains

Julia M. Khalack[1,2,*] and M. J. Velgakis[1,†]
[1]*Engineering Science Department, University of Patras, 26110 Patras, Greece*
[2]*Bogolyubov Institute for Theoretical Physics, 03143 Kyiv, Ukraine*
(Received 2 September 2001; published 18 March 2002)

We consider rotational motion of protons within a hydrogen-bonded zig-zag chain. Each proton is subjected to a Coulomb interaction from the three nearest heavy ions, as well as from the two neighboring protons. The hydrogen bonding is modeled with an additional double-minimum on-site potential. The system admits discrete breather solutions in the gap below the phonon band. The numerically exact procedure using an anticontinuum limit is exploited to obtain these solutions, which appear to be asymmetric due to the asymmetry of the interaction potential. Only single-well orbits are considered. A linear stability analysis is performed. The discrete breather solutions are shown to be linearly stable provided the nonresonance condition is satisfied, and they turn out to be unstable in the region of 2:3 parametric resonance. Phonon-breather solutions are found in the 1:2 resonance region. Two kinds of two-site breather solutions are investigated.

DOI: 10.1103/PhysRevE.65.046604 PACS number(s): 45.05.+x, 63.20.−e, 05.45.−a, 82.30.Rs

I. INTRODUCTION

Discrete breathers or time-periodic intrinsically localized modes in translationally invariant lattices of nonlinear coupled oscillators were discovered as early as in 1970 by Ovchinnikov [1]. However, they gained much attention from the physics community after their rediscovery by Sievers *et al*. in 1988 [2,3], when the phenomenon was realized to be of great generality in lattices. Intrinsic localized modes can be found in any weakly coupled discrete nonlinear system (see Ref. [4] for a review) provided nonresonance condition is satisfied. Both discreteness and nonlinearity are equally important. Discreteness gives bounded character of phonon spectrum, while nonlinearity is responsible for frequency dependence of vibration amplitudes. The existence of discrete breathers as time-periodic solutions of nonlinear lattice equations under quite general conditions is proven by rigorous theorems [5,6], and numerical schemes for their explicit calculation are developed [7]. Recently, discrete breathers were experimentally observed in coupled optical waveguides [8,9], in charge-density wave systems [10], in magnetic systems [11], in arrays of coupled Josephson junctions [12,13], and possibly in myoglobin [14]. Hydrogen-bonded systems such as ice, quasi-one-dimensional hydrogen-bonded crystals, and one-dimensional hydrogen-bonded chains (see Ref. [15] for a review) represent another type of condensed matter systems in which discrete breathers could possibly exist and could be detected experimentally.

A hydrogen-bonded chain can be considered as a zig-zag network of heavy ions intermediated with protons, each of the protons being linked to one of its neighbor heavy ions with a (shorter) covalent bond, and to another neighbor heavy ion with a (longer) hydrogen bond. Ground state of such a system is usually doubly degenerate with respect to the left or right covalent bond. A transition between these two ground states can be realized by means of ionic (also hopping) or orientational (also bonding or Bjerrum) defects [16]. The first one incorporates a proton hopping between two energy minima in intrabond with an interchange of covalent and hydrogen links, and the second one takes place through a molecule rotation as a whole with a break and successive renovation of hydrogen bond.

A number of one- and two-component one-dimensional models has been introduced to investigate the dynamics of ionic [17–21] and orientational [22–24] or even both [25–28] of these soliton type excitations, which are believed to be of great importance in the process of proton transfer [15,16]. However, the discrete breathers in hydrogen-bonded chains have been studied only for strong hydrogen bonding [29] with nondegenerate ground state. This case falls into a more general class of one-dimensional diatomic Fermi-Pasta-Ulam lattices for which the discrete breather solutions of different symmetry can exist [30–38], in the frequency gap between optical and acoustic phonon bands, as well as above the optical band.

As to the weakly coupled hydrogen-bonded chains, in the limit of infinite heavy ion masses the properties of the discrete breather solutions concerned with intrabond proton motions can be roughly understood with the help of the Klein-Gordon model with double-well potential (see, e.g., Refs. [39,41,42]), where the discrete breathers can exist in the gap below the phonon band. The discrete breathers concentrated on rotational proton motion are somewhat different from the previous ones because of another form (namely, periodicity) of the proton on-site potential and more complicated (nonharmonic) proton-proton interaction due to a strong change in the system geometry upon reorientation of the chain molecules. In the present paper we consider the simplest case of orientational discrete breathers with single-well proton orbits, the effect of on-site potential double-well character and periodicity being kept for future investigations.

II. MODEL

We consider a network of protons in a two-dimensional zig-zag chain of infinitely massive heavy ions (see Fig. 1).

*Email address: julia@nonlin.bitp.kiev.ua
†Corresponding author.
Email address: velgakis@terpsi.iceht.forth.gr

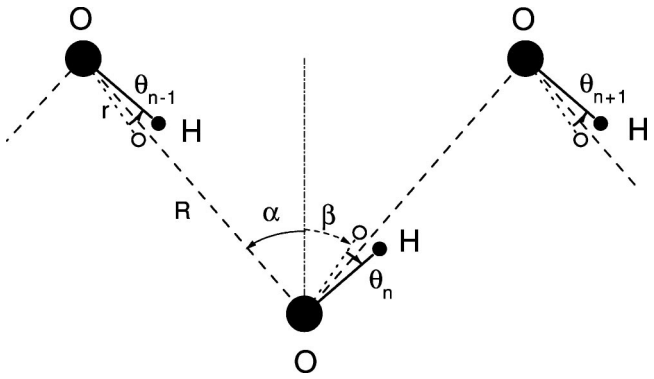

FIG. 1. A schematic representation of the system geometry. Equilibrium proton positions are shown with open circles. Big filled circles represent heavy ions (oxygens).

Each proton is coupled to one of the neighbor heavy ions with a covalent bond with its length being fixed at r. Then the position of the nth proton is determined uniquely by the angle θ_n measured from the proton equilibrium position to the right from its heavy ion (given with the angle β).

The Hamiltonian function for the protonic subsystem has a form

$$H=\sum_n \left\{\frac{I}{2}\dot{\theta}_n^2+V(\theta_n)+U_1(\theta_n)+U_2(\theta_n,\theta_{n+1})\right\}, \quad (1)$$

where the first term gives the kinetic energy of proton, and $I=mr^2$ is the proton moment of inertia. To take into account the double-well character of the on-site potential modeling hydrogen bonding, the second term in Eq. (1) was chosen in the form

$$V(\theta_n)=K[\cos(\beta+\theta_n)-\cos\alpha]^2, \quad (2)$$

where the angle α is defined by the geometry of the heavy ion zig-zag backbone (see Fig. 1), and the parameter K gives the barrier height for the on-site potential. The last two terms in Eq. (1) describe the Coulomb interaction of the nth proton with its neighbor heavy ions and protons, respectively,

$$U_1(\theta_n)=-\frac{q^2}{4\pi\varepsilon_0 R}\left[\frac{1}{\sqrt{1+\rho^2-2\rho\cos(\alpha-\beta-\theta_n)}}+\frac{1}{\sqrt{1+\rho^2-2\rho\cos(\alpha+\beta+\theta_n)}}\right], \quad (3)$$

and

$$U_2(\theta_n,\theta_{n+1})=\frac{q^2}{4\pi\varepsilon_0 R}\{[\sin\alpha+\rho\sin(\beta+\theta_{n+1})-\rho\times\sin(\beta+\theta_n)]^2+[\cos\alpha-\rho\cos(\beta+\theta_{n+1})-\rho\cos(\beta+\theta_n)]^2\}^{-1/2}, \quad (4)$$

where q is the effective electric charge of the proton in the chain molecule, R is the distance between neighbor heavy ions (see Fig. 1), and $\rho=r/R$ is the reduced covalent bond length.

For the numerical simulations we use the parameter values given by Kryachko and Sokhan [22] for orientational defect on ice: $r=0.94$ Å, $2\alpha=109.5°$, $R=2.76$ Å, $q=0.6e$, and the barrier height for on-site dipole rotation $U_B^{(0)}=7.68$ Kcal/mol. Since the parameter $\rho\approx 0.3$, we consider the dipole-dipole approximation used in Refs [23,24] to be inapplicable to our case and therefore retain the general form of interaction (3),(4).

The parameter K for hydrogen bonding on-site potential is chosen to give the value $U_B^{(0)}$ per site for simultaneous rotation of all hydrogens by $\theta_n=-\beta$. It gives

$$U_B^{(0)}=K(1-\cos\alpha)^2-K(\cos\beta-\cos\alpha)^2+\frac{q^2}{4\pi\varepsilon_0 R}\left[\frac{1}{\sqrt{1+4\rho^2-4\rho\cos\alpha}}-\frac{2}{\sqrt{1+\rho^2-2\rho\cos\alpha}}-\frac{1}{\sqrt{1+4\rho^2\cos^2\beta-4\rho\cos\alpha\cos\beta}}+\frac{1}{\sqrt{1+\rho^2-2\rho\cos(\alpha-\beta)}}+\frac{1}{\sqrt{1+\rho^2-2\rho\cos(\alpha+\beta)}}\right]. \quad (5)$$

Then K can be found as

$$K=\left\{U_B^{(0)}-\frac{q^2}{4\pi\varepsilon_0 R}\left[\frac{1}{\sqrt{1+4\rho^2-4\rho\cos\alpha}}-\frac{2}{\sqrt{1+\rho^2-2\rho\cos\alpha}}-\frac{1}{\sqrt{1+4\rho^2\cos^2\beta-4\rho\cos\alpha\cos\beta}}+\frac{1}{\sqrt{1+\rho^2-2\rho\cos(\alpha-\beta)}}+\frac{1}{\sqrt{1+\rho^2-2\rho\cos(\alpha+\beta)}}\right]\right\}\Big/(1-2\cos\alpha-\cos^2\beta+2\cos\alpha\cos\beta). \quad (6)$$

The equilibrium angle β is chosen to minimize the Hamiltonian (1) upon $\theta_n\equiv 0$,

$$\frac{\partial}{\partial\beta}[V(\beta;0)+U_1(\beta;0)+U_2(\beta;0,0)]=0. \tag{7}$$

The approximate value of β can be found as

$$\beta=\alpha-\frac{\{\partial[V(\beta;0)+U_1(\beta;0)+U_2(\beta;0,0)]/\partial\beta\}_{\beta=\alpha}}{\{\partial^2[V(\beta;0)+U_1(\beta;0)+U_2(\beta;0,0)]/\partial\beta^2\}_{\beta=\alpha}}. \tag{8}$$

For our choice of potentials (2),(3),(4) we get

$$\{\partial[V(\beta;0)+U_1(\beta;0)+U_2(\beta;0,0)]/\partial\beta\}_{\beta=\alpha}$$
$$=\frac{q^2}{4\pi\varepsilon_0 R}\left\{\frac{\rho(2\rho-1)\sin 2\alpha}{[1-4\rho(1-\rho)\cos^2\alpha]^{3/2}}+\frac{\rho\sin 2\alpha}{[1+\rho^2-2\rho\cos 2\alpha]^{3/2}}\right\} \tag{9}$$

and

$$\{\partial^2[V(\beta;0)+U_1(\beta;0)+U_2(\beta;0,0)]/\partial\beta^2\}_{\beta=\alpha}$$
$$=\frac{2\sin^2\alpha}{(1-\cos\alpha)^2}\left\{U_B^0-\frac{q^2}{4\pi\varepsilon_0 R}\left[\frac{1}{[1-4\rho(\cos\alpha-\rho)]^{1/2}}-\frac{2}{[1+\rho^2-2\rho\cos\alpha]^{1/2}}-\frac{1}{[1-4\rho(1-\rho)\cos^2\alpha]^{1/2}}+\frac{1}{1-\rho}+\frac{1}{[1+\rho^2-2\rho\cos 2\alpha]^{1/2}}\right]\right\}$$
$$+\frac{q^2}{4\pi\varepsilon_0 R}\left\{\frac{3\rho^2(2\rho-1)^2\sin^2 2\alpha}{[1-4\rho(1-\rho)\cos^2\alpha]^{5/2}}+\frac{2\rho(2\rho\cos 2\alpha-\cos^2\alpha)}{[1-4\rho(1-\rho)\cos^2\alpha]^{3/2}}+\frac{\rho}{(1-\rho)^3}-\frac{3\rho^2\sin^2 2\alpha}{[1+\rho^2-2\rho\cos 2\alpha]^{5/2}}+\frac{\rho\cos 2\alpha}{[1+\rho^2-2\rho\cos 2\alpha]^{3/2}}\right\}. \tag{10}$$

Equation (8) gives the approximate value of correction $\alpha-\beta\approx 0.0294$, while the exact difference is $\alpha-\beta=0.023\,747$. The on-site potentials (2) and (3) for this choice of β are shown in Fig. 2(a) with the curves 1 and 2, and the form of the interaction term (4) is presented in Fig. 2(b).

III. ANTICONTINUUM LIMIT AND PHONON BAND

To obtain numerically [7] the discrete breather solutions using the proof of existence by MacKay and Aubry [5], we

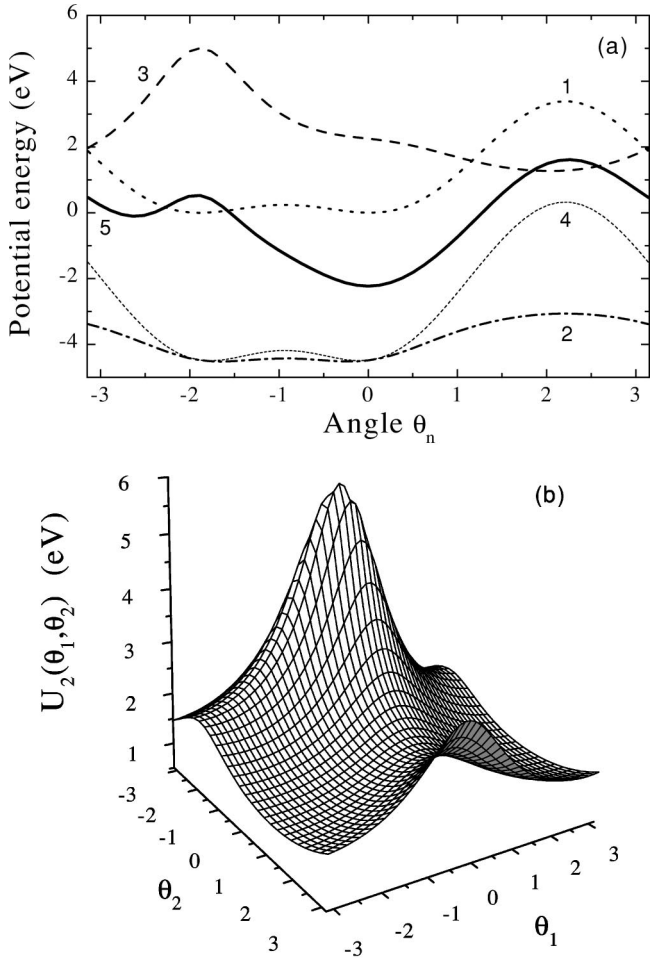

FIG. 2. (a) The potential energy profiles for the different kinds of interaction. 1, hydrogen bonding energy $V(\theta_n)$; 2, Coulomb interaction $U_1(\theta_n)$ with neighboring oxygens; 3, the effective proton-proton interaction potential $U_2^{(0)}(\theta_n)$ for the anticontinuum limit; 4, $V(\theta_n)+U_1(\theta_n)$; 5, $V(\theta_n)+U_1(\theta_n)+U_2^{(0)}(\theta_n)$. (b) The proton-proton interaction energy $U_2(\theta_n,\theta_{n+1})$. In this work all angles are measured in radians.

introduce the anticontinuum limit into the system Hamiltonian. Despite the resemblance of our system to the Klein-Gordon chain, it does not suffice simply to insert a factor of C (called a coupling constant) into the interaction term (4) because of the change of the proton equilibrium angle β. Luckily, an idea of great help suggested for Fermi-Pasta-Ulam chain [43] is to insert an additional on-site potential of the form $(1-C)U_2(\theta_n,0)$ into the system Hamiltonian:

$$H^m(C)=\sum_n\left\{\frac{I}{2}\dot\theta_n^2+V(\theta_n)+U_1(\theta_n)+(1-C)U_2^{(0)}(\theta_n)+CU_2(\theta_n,\theta_{n+1})\right\}. \tag{11}$$

But in our case the effective on-site potential $U_2^{(0)}(\theta_n)$ has to be chosen to compensate the missing energy of interaction

with the two [$(n-1)$-th and $(n+1)$-th] neighboring protons rested at their equilibrium positions. Hence,

$$U_2^{(0)}(\theta_n) = U_2(\theta_n,0) + U_2(0,\theta_n) - U_2(0,0)$$
$$= \frac{q^2}{4\pi\varepsilon_0 R}[-[\sin^2\alpha + (\cos\alpha - 2\rho\cos\beta)^2]^{-1/2}$$
$$+ (\{\sin\alpha + \rho[\sin\beta - \sin(\beta+\theta_n)]\}^2$$
$$+ \{\cos\alpha - \rho[\cos\beta - \cos(\beta+\theta_n)]\}^2)^{-1/2}$$
$$+ (\{\sin\alpha - \rho[\sin\beta - \sin(\beta+\theta_n)]\}^2$$
$$+ \{\cos\alpha - \rho[\cos\beta - \cos(\beta+\theta_n)]\}^2)^{-1/2}], \tag{12}$$

the last term being added to keep the ground-state energy of the system fixed with the change of C. The form of this effective on-site potential is represented in Fig. 2(a) by curve 3. The equations of motion to be solved are

$$I\ddot{\theta}_n + \frac{dV(\theta_n)}{d\theta_n} + \frac{dU_1(\theta_n)}{d\theta_n} + (1-C)\left(\frac{\partial U_2(\theta_n,0)}{\partial\theta_n} + \frac{\partial U_2(0,\theta_n)}{\partial\theta_n}\right) + C\left(\frac{\partial U_2(\theta_n,\theta_{n+1})}{\partial\theta_n} + \frac{\partial U_2(\theta_{n-1},\theta_n)}{\partial\theta_n}\right) = 0. \tag{13}$$

It is obvious that for a coupling constant $C=0$ with a resulting on-site potential given by curve 5 in Fig. 2(a), we have a system of decoupled nonlinear oscillators, and for $C=1$ we get the realistic system (1) with a general interaction term (4).

The phonon band of the system can be found from the linearized Hamiltonian

$$H_0 = I\sum_n \left\{\frac{1}{2}\dot{\theta}_n^2 + \Omega_0^2\frac{\theta_n^2}{2} + C\Omega_0^2\chi\theta_n\theta_{n+1}\right\}, \tag{14}$$

with

$$\Omega_0^2 = \frac{1}{I}\left.\frac{\partial^2[V(\theta_n) + U_1(\theta_n) + U_2^{(0)}(\theta_n)]}{\partial\theta_n^2}\right|_{\theta_n=0}$$

and

$$\chi = \frac{1}{I\Omega_0^2}\frac{\partial^2 U_2(\theta_n,\theta_{n+1})}{\partial\theta_n\partial\theta_{n+1}}_{\theta_n=\theta_{n+1}=0}. \tag{15}$$

It is clearly seen that our choice of introducing anticontinuum limit does not change equilibrium positions of protons. Moreover, the frequency of harmonic vibrations Ω_0^2 does not depend on C, so we have no problem with intersecting the dangerous resonance region when increasing C at constant value of breather frequency (cf. Refs. [29,34,38]). Introducing the dimensionless time variable $\tau=\Omega_0 t$, the linearized equations of motion take the form

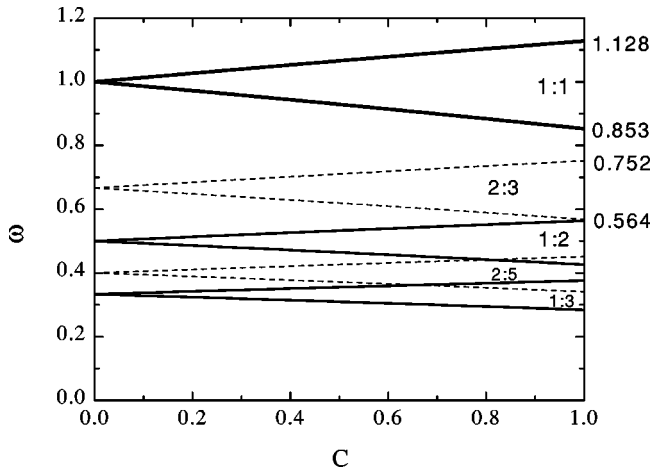

FIG. 3. The dependence of phonon band frequencies on the coupling constant C (upper two solid lines). The regions of 1:2 and 1:3 resonance with phonon band are also shown with solid lines. The regions of parametric resonance are given with dashed lines. Regions of higher-order resonances in the lower part of the gap are not shown.

$$\ddot{\theta}_n + \theta_n + C\chi(\theta_{n-1} + \theta_{n+1}) = 0. \tag{16}$$

The phonon spectrum can be found with the help of the ansatz: $\theta_n = A\exp[i(\omega t - kn)]$; substituted into Eq. (16) it gives $\omega^2 = 1 + 2C\chi\cos k$ with the lower and higher band edges

$$\omega_{min} = \sqrt{1-2C|\chi|}, \quad \omega_{max} = \sqrt{1+2C|\chi|}. \tag{17}$$

For our original system (1) we have $C=1$ and

$$\omega_{min} = 0.852756, \quad \omega_{max} = 1.128187. \tag{18}$$

The dependence of the phonon band on the coupling constant C is shown in Fig. 3 (phonon band is labeled with 1:1 resonance). The regions of 1:2 and 1:3 resonance with phonon band are shown with solid lines, and the regions of 2:3 and 2:5 parametric resonance are given by dashed lines. Higher-order resonance regions are not shown. The stable discrete breather solutions are expected to be found in the gap below the phonon band and above the 2:3 parametric resonance region. All the frequencies below the 1:3 resonance region have higher-order harmonics in the phonon spectrum.

IV. NUMERICAL RESULTS

The numerically exact time-reversible discrete breather solutions considered in this section have been obtained from the anticontinuum limit with the help of the Newton-Raphson method [7] with periodic boundary conditions imposed. In the most cases we have used a chain length N of about 25 particles, unless stated otherwise. Since we are interested in the discrete breather solutions to the system (1), only the results for $C=1$ are reported.

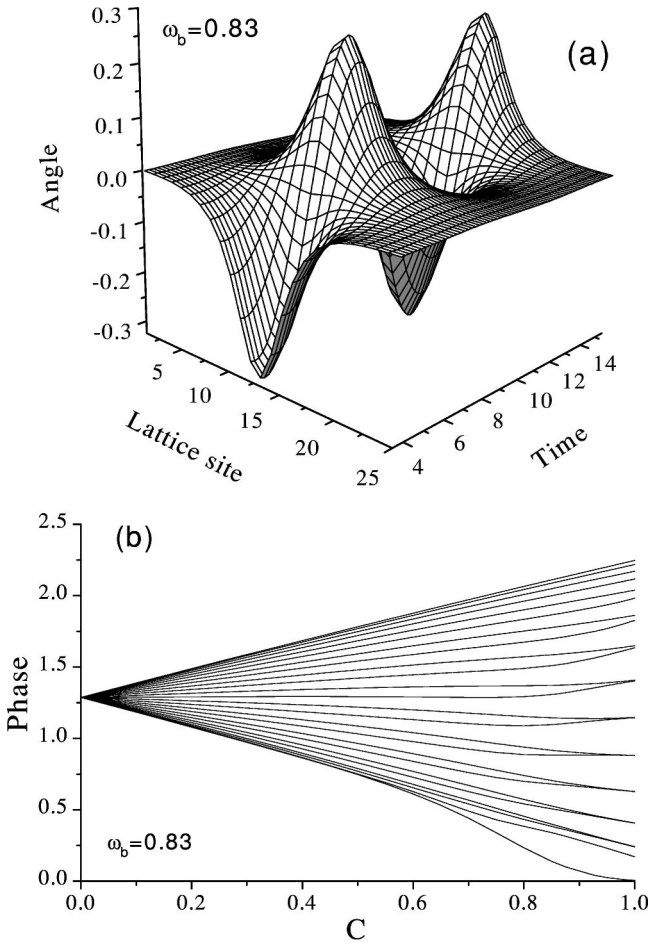

FIG. 4. (a) Time dependence of the discrete breather solution for $\omega_b=0.83$ (just below the lower edge of the phonon band). (b) Evolution of Floquet eigenvalues along the unit circle with the increase of the coupling C.

A. Single-site breather solutions

As mentioned above, discrete breather solutions are proven to exist in weakly coupled systems provided nonresonance condition is satisfied. The last condition means that none of the higher-order harmonics of the breather frequency ω_b is allowed to be in resonance with a phonon spectrum. Therefore, the frequency regions $[\omega_{min}/n, \omega_{max}/n]$ with $n=1,2,3,\ldots$, are to be excluded from considerations.

In the case of our system with the phonon band given by Eq. (17) the nonresonance condition is satisfied for the frequency range $0.564\,10<\omega_b<0.852\,76$ $(\omega_{max}/2<\omega_b<\omega_{min})$ and $0.376\,06<\omega_b<0.426\,38$ $(\omega_{max}/3<\omega_b<\omega_{min}/2)$. However, for the coupling constant $C=1$ the localized one-site discrete breather solutions have been found only for the first frequency range.

Figure 4(a) represents the form of discrete breather solution for $\omega_b=0.83$, which is close to the lower edge of the phonon band, from which this solution bifurcates. The stability analysis of this solution shows that all the Floquet eigenvalues lie on the unit circle. The dependence of their phases on the coupling parameter C is plotted in Fig. 4(b).

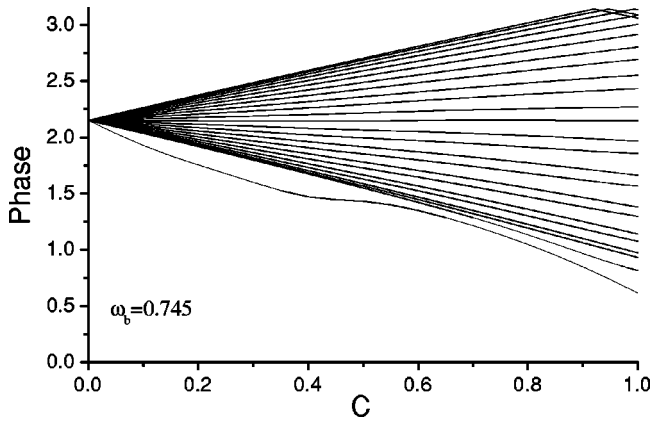

FIG. 5. Evolution of Floquet eigenvalues for a discrete breather solution from the middle of the gap between two resonance regions ($\omega_b=0.745$). Note overlapping of two band images at π.

Upon decreasing the breather frequency ω_b the solution remains stable down to some frequency for which a collision of Floquet eigenvalues at -1 takes place. The exact value of collision frequency slightly depends on the system size N. For $N=25$ it is $\omega_b=0.751\,37$, and for $N\to\infty$ it approaches $2\omega_{max}/3=0.752\,12$. Such a collision gives rise to some instabilities, but does not prevent one from continuation of the breather solution. Figure 5 represents a typical evolution of the Floquet eigenvalues on the unit circle upon increase of the coupling parameter C for the breather frequency just below $2\omega_{max}/3$. Overlapping with complex conjugate image of the band can be observed in the right upper corner of Figure 5 (only the eigenvalues with positive imaginary part are plotted, therefore, it looks like reflection at π). For the frequencies under consideration instabilities appear as a result of collision of the Floquet eigenvalues of extended modes. These instabilities represent a finite size effect [40] and shrink with the growth of the chain length. On the other hand, a finite chain length is the reason that for most of the frequencies ω_b there are no coinciding Floquet eigenvalues at $C=1$, and the discrete breather solution is stable (as for the case of $\omega_b=0.745$ represented at Fig. 5).

The behavior of Floquet eigenvalues becomes more interesting after the breather frequency falls below 2/3, when the band passes through -1 at $C=0$. In this case the localized mode starts detaching from the band in the upward direction, and meets its complex conjugate at -1, yielding a period-doubling bifurcation. Then the pair of Floquet eigenvalues have an excursion apart from -1 along a real axis and comes back to -1 at some value of C. After that the pair of eigenvalues moves along the unit circle and gives rise to Hopf-like instability when it reaches the leading edge of the phonon band. Such a behavior is illustrated in Fig. 6(a)–(b), where the evolution of Floquet eigenvalues with C for $\omega_b=0.62$ is shown. Additional small instabilities observed in Fig. 6(b) are due to collision of extended modes.

Evolution of the initial breather profile with the decrease of ω_b is presented in Fig. 7. The asymmetry of the single-site discrete breather initial profile is clearly seen from Fig. 7(a), where the central part of the breather is shown. The amplitude of oscillation of the left neighbor to the central particle

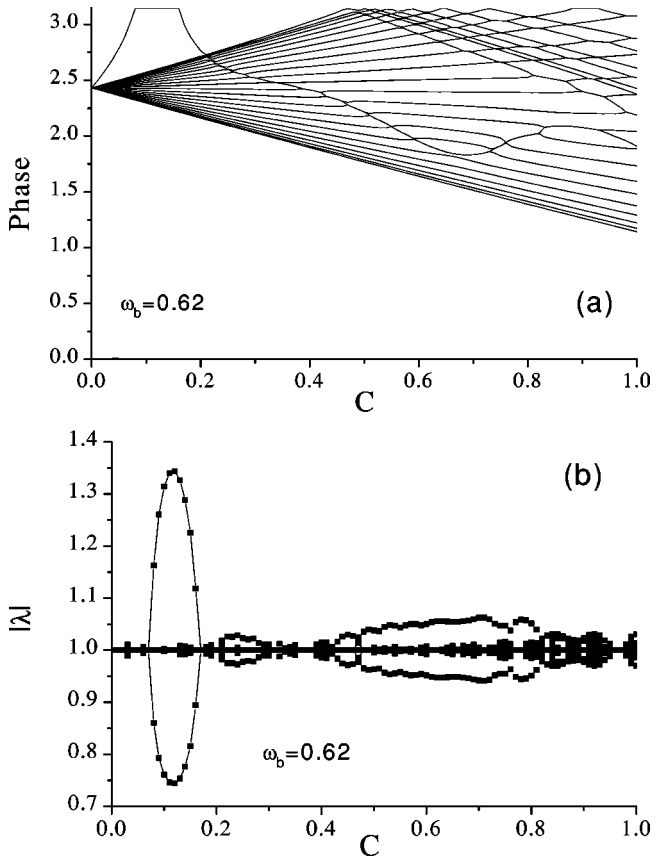

FIG. 6. The stability analysis for the discrete breather solution with $\omega_b=0.62$: the phases (a) and the absolute values (b) of Floquet eigenvalues as a function of coupling C.

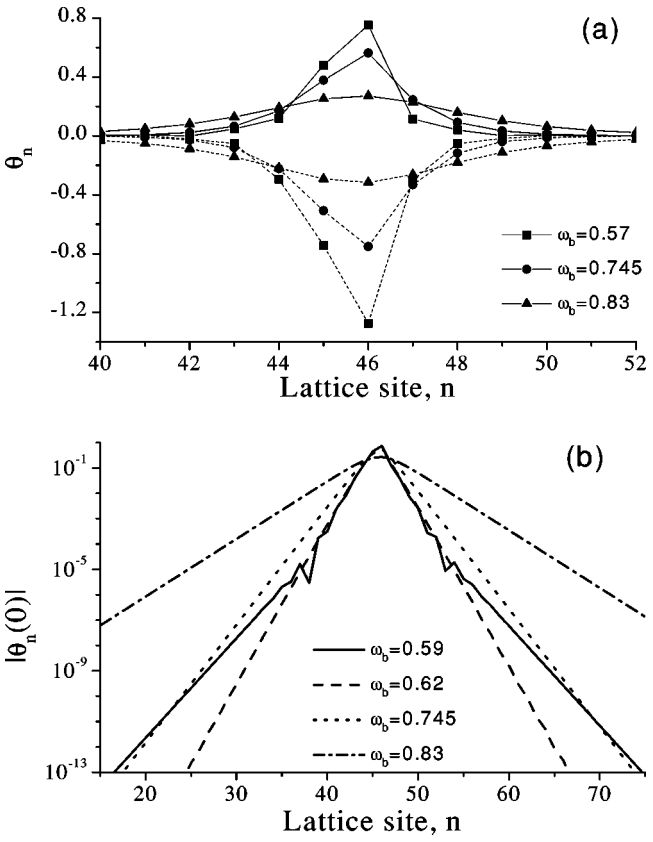

FIG. 7. (a) The profiles of the discrete breather solutions at $\tau=0$ (solid lines) and $\tau=\pi/\omega_b$ (dashed lines) for three different frequencies: $\omega_b=0.57$ (squares), $\omega_b=0.745$ (circles), $\omega_b=0.83$ (triangles). (b) The initial profiles of the discrete breather solutions in semilogarithmic scale for the frequencies $\omega_b=0.59$ (solid line), $\omega_b=0.62$ (dashed line), $\omega_b=0.745$ (dotted line), and $\omega_b=0.83$ (dash-dotted line); $N=90$. The solution with $\omega_b=0.62$ has the least localization length, because its frequency is very close to the critical one $\omega_c\approx 0.6325$.

is always higher than the amplitude of oscillation of the right neighbor particle. We are not aware of the similar result for the Klein-Gordon chains with interaction of the form $W(\theta_{n+1}-\theta_n)$. Therefore, we believe that this asymmetry is due to the more general form of interaction potential $U_2(\theta_n,\theta_{n+1})$ used here.

The exponential character of discrete breather solution localization is proved with Fig. 7(b) (note a semilogarithmic scale). Two localization lengths are clearly seen for the frequencies $\omega_b<0.6$ because of the tails oscillations at the frequency $2\omega_b$.

Let us find the localization lengths for oscillations with frequencies $l\omega_b$ ($l=1,2,3,\ldots$). An ansatz $\theta_n^{(l)}=A_l|\zeta_l|^n e^{il\omega_b t}$, being substituted into the Eq. (16) with $C=1$, gives

$$-l^2\omega_b^2+1+\chi(\zeta_l^{-1}+\zeta_l)=0, \tag{19}$$

so that

$$\zeta_l=\frac{-(1-l^2\omega_b^2)\pm\sqrt{(1-l^2\omega_b^2)^2-4\chi^2}}{2\chi}. \tag{20}$$

For exponentially localized solutions we have to adopt $|\zeta_l|<1$ as $n\to+\infty$. Therefore, for the frequency range $\omega_{max}/2<\omega_b<\omega_{min}$ and for $\chi=-0.136<0$,

$$\zeta_1=\frac{-(1-\omega_b^2)+\sqrt{(1-\omega_b^2)^2-4\chi^2}}{2\chi}>0 \tag{21}$$

and

$$\zeta_2=\frac{4\omega_b^2-1-\sqrt{(4\omega_b^2-1)^2-4\chi^2}}{2\chi}<0. \tag{22}$$

It is easy to check that at $\omega_c=\sqrt{2/5}\approx 0.6325$ both localization lengths are equal ($\zeta_1=-\zeta_2$), and below this frequency $|\zeta_2|>|\zeta_1|$ (see Fig. 8). This means that the first Fourier harmonics decays faster than the second one, and at some distance from the breather center the oscillations become dominated with the harmonics with the largest absolute value of ζ_l [44] ($l=2$ for our case), resulting in antiphase character of neighbor particle oscillations ($\zeta_2<0$), what was the reason for plotting absolute value $|\theta_n(0)|$ in Fig. 7(b). For the frequencies close to ω_c [$\omega_b=0.62$ in Fig. 7(b)] both localization lengths are close to each other, therefore, domination of the second harmonics is not very pronounced and can be observed only for long chains. At these frequencies the dis-

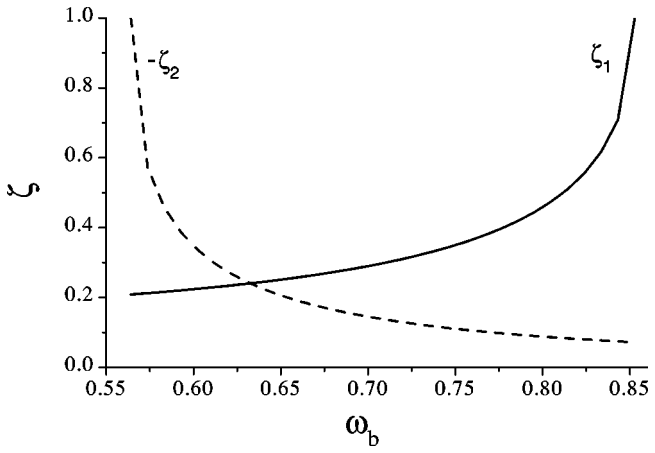

FIG. 8. The dependence of localization parameters $\zeta_{1,2}$ on the breather frequency ω_b.

crete breather solution is mostly localized because of the minimum of overall decay factor $\max(|\zeta_1|,|\zeta_2|)$ (see Fig. 8).

Figure 8 shows that for the breather frequency ω_b approaching $\omega_{max}/2$ the absolute value $|\zeta_2|\to 1$, and the second harmonics tends to be delocalized, while the first harmonics oscillations remain localized with $\zeta_1 \approx 0.2$. As a result, upon decreasing the frequency below the value of $\omega_{max}/2$ the discrete breather solution evolves into the phonon-breather solution with the central part oscillating at the frequency ω_b, and the rest of the chain performing nondecaying $2\omega_b$ out-of-phase oscillations (see Fig. 9).

Phononbreather solution is unstable because of the Hopf-like instability from collision of localized mode with the phonon band [cf. Figs. 6(a), 6(b)], but the main instability at $C=1$ comes from the 1:2 resonance with the phonon band. The appearance of the last instability can be observed in the right lower corner of Fig. 9(b) as a collision of the Floquet eigenvalues corresponding to the extended modes with the time shift mode eigenvalue at $+1$. An energy of the phonon-breather solution diverges linearly with a system size N: $E_{ph\text{-}b}(N)=E_b^0+\kappa N$. An out-of-phase character of phonon oscillations leads to a dependence of a breather part E_b^0 on the parity of the system size N. For example, for the case of $\omega_b=0.55$ we have $E_{ph-b}^{odd}(N)=0.488\,919\,4+0.126\,199\,6N$ for odd N, and $E_{ph-b}^{even}(N)=0.545\,480\,5+0.126\,199\,6N$ for even N.

The amplitudes of the central particle displacements and the values of the breather energy for the whole frequency range (including obtained phononbreather solutions) are summarized in Figs. 10(a), 10(b). It is clearly seen that the discrete breather solution originates from the lower edge of the phonon band.

The single-site discrete breather solutions with the frequency from the lower allowed range ($\omega_{max}/3<\omega<\omega_{min}/2$) could not be continued up to the value of the coupling constant $C=1$. The reason is most probably the low computer precision for the Newton method to follow single-well breather solution with the initial (or final, for $\tau=\pi/\omega_b$) central particle displacement at the top of the potential barrier between two neighbor wells. Some modification of computational technique is required to answer the question of existence of discrete breather solutions in this low-frequency region. Most probably, the answer is negative, because the abrupt decrease of the step in coupling parameter C has been observed in our simulations already for $C=0.1/0.2$ for all nonresonant low frequencies. Remarkably, that at this failure of the Newton method the isolated Floquet eigenvalue corresponding to localized mode is located at the unit circle and has the phase of about 0.2, so it is not the case of bifurcation associated with a collision at $+1$.

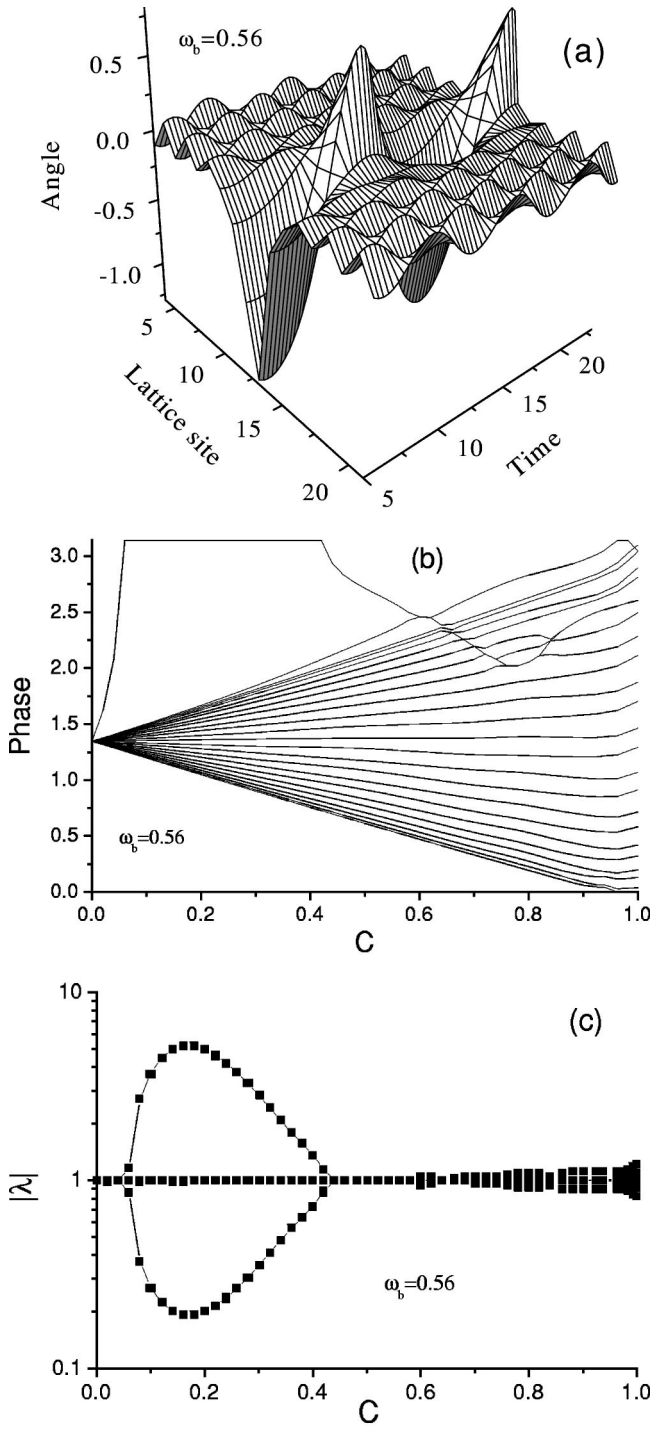

FIG. 9. Phonon-breather solution for $\omega_b=0.56$ (a) and its stability analysis (b,c).

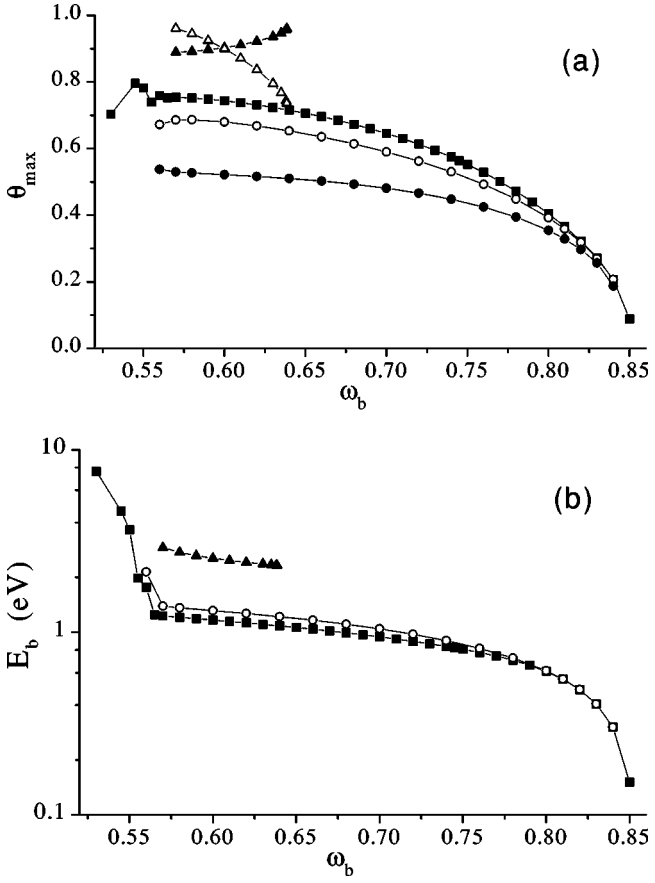

FIG. 10. (a)The maximum positive displacements of the central particles of one-site (squares), two-site in-phase (circles), and two-site out-of-phase (triangles) breather as a function of breather frequency ω_b. For the two-site breathers the open symbols show the displacement of the left central particle, and the filled ones stand for the right particle displacement. (b) The frequency dependence of the energy of one-site (squares), two-site in-phase (circles), and two-site out-of-phase (triangles) breather. Attention should be paid to the semilogarithmic scale.

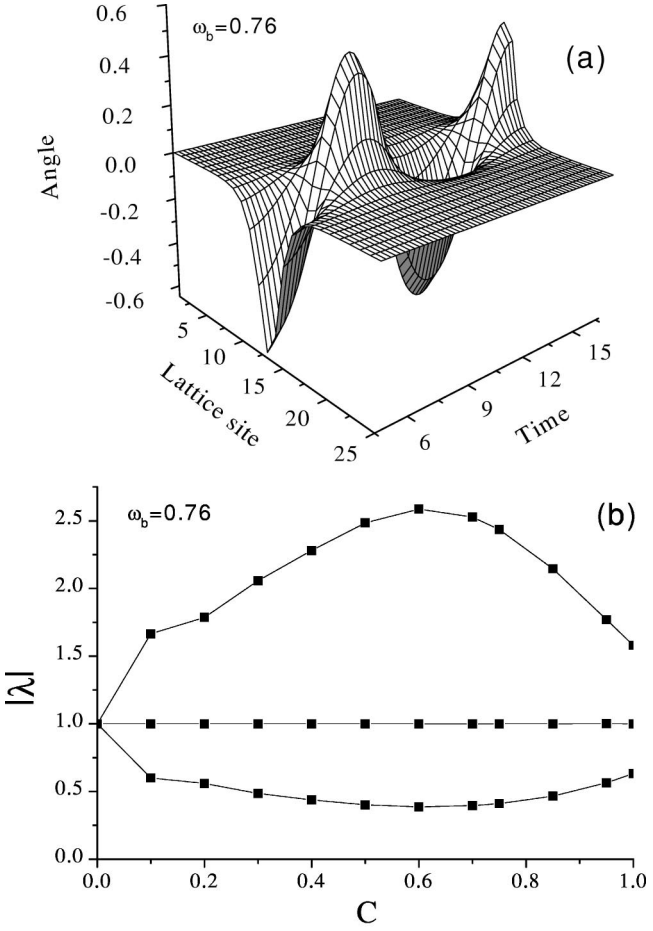

FIG. 11. A two-site in-phase discrete breather solution (a) and its stability analysis (b) for $\omega_b = 0.76$.

As a result of a finite precision of calculations, the solutions other than low-frequency single-well discrete breather solutions (double-frequency single-well solutions, solutions with the central particle being trapped in the secondary potential well or performing large-amplitude two-well oscillations) could have been found for $C=1$ depending on the sign of the central particle initial displacement at $C=0$. The obtained double-well solutions are beyond of the scope of the present paper and can be a subject for more detailed future investigations.

B. Multibreather solutions

Two kinds of two-site breather solutions were obtained in the frequency range $0.565 \leqslant \omega_b \leqslant 0.85$. The in-phase two-site discrete breather solution originating from the coding sequence (. . . ,0,0,1,1,0,0, . . .) [45] and shown in Fig. 11(a) was found to exist and to be unstable for all the frequencies from this range. The stability analysis [see Fig. 11(b)] shows that the main instability comes from the pair of Floquet eigenvalues moving on the real axis from $+1$ (we don't report additional small instabilities for $\omega_b < 2\omega_{max}/3$, which have the same nature as for the one-site discrete breather). The bigger Floquet eigenvalue is always real and grows from 1.00 (the matter of precision of eigenvalue calculation) at $\omega_b = 0.85$ to 9.12 at $\omega_b = 0.57$.

Due to the asymmetry of the interaction potential (4) the left excited particle of a two-site in-phase breather solution has a higher oscillation amplitude than the right one. Therefore, the initial profile for this two-site breather has a maximum at only one of the chain sites, as in the case of the one-site solution. The only difference is that the amplitude of the right (this time excited) neighbor to the central particle is higher than the amplitude of the left (nonexcited) one. The frequency dependence of initial displacements for the two central particles and of the breather energy are shown in Figs. 10(a) and 10(b), respectively.

The two-site out-of-phase breather solutions with originating coding sequence (. . . ,0,0,$-$1,1,0,0, . . .) were found to exist at $C=1$ only in the frequency range $0.57 \leqslant \omega_b \leqslant 0.6385$ (at higher frequencies the solution could not be continued to $C=1$ because of the collision with localized mode at $+1$). The form of the solution and its stability analy-

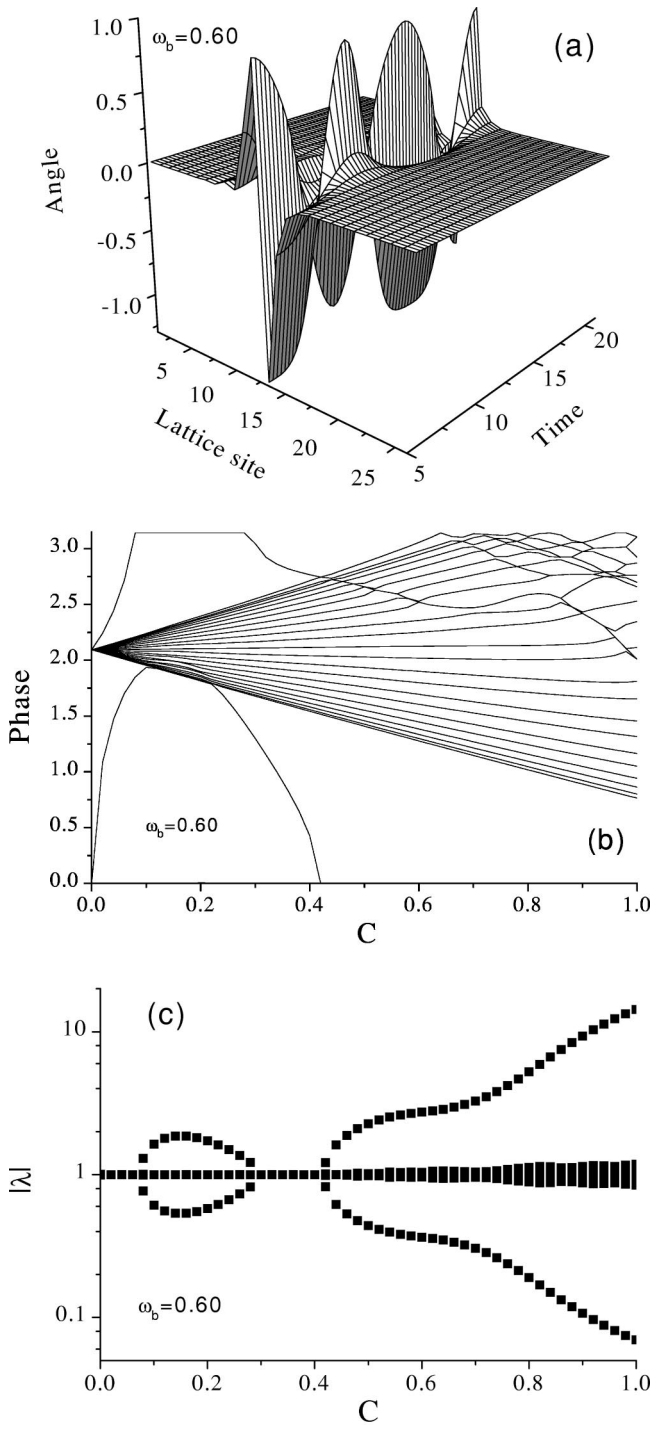

FIG. 12. A two-site out-of-phase discrete breather solution (a) and its stability analysis (b,c) for $\omega_b = 0.60$.

sis are represented at Figs. 12(a)–(c). The solution is unstable for $C=1$ for all frequencies it exists, the largest Floquet eigenvalue ranging from 4.29 at $\omega_b = 0.6385$ to 39.30 at $\omega_b = 0.57$. But this solution can be stable at the small values of the coupling parameter C, as it is illustrated by Fig.12c (cf. the stability of out-of-phase two-site breather in Klein-Gordon chain with the soft potential [39] and instability of antisymmetric mode centered on heavy particle for β-FPU chain [43]). The initial profile for this breather has no definite symmetry. Nor the maximum positive displacements of two central particles have definite ratio. Both the maximum displacements are depicted in Fig. 10(a). The energy of this breather [depicted in Fig. 10(b)] is larger than the energy of in-phase two-site breather.

V. SUMMARY AND OUTLOOK

In this paper we have investigated the rotational motion of molecules in a zig-zag hydrogen-bonded chain. Using the numerically exact procedure, we have obtained single-well orientational discrete breather solutions starting from the anticontinuum limit.

The one-component system considered is characterized by nonlinear on-site potential and nonlinear interaction term, dependent not only on the difference $(\theta_{n+1} - \theta_n)$, but also on both angles. Although this system cannot be restricted to the pure case of Klein-Gordon or Fermi-Pasta-Ulam chain, it reveals the features of both. Therefore, we were urged to use a proper modification of the two corresponding ways of introducing the anticontinuum limit into the system Hamiltonian.

The system admits discrete breather solutions with the frequencies in the gap between the phonon band and the region of 1:2 resonance. These solutions bifurcate from the lower edge of the phonon band and have asymmetric profile due to the more general character of interaction potential. They are stable down to the breather frequencies entering the parametric 2:3 resonance region. A presence of two localization lengths is clearly seen for discrete breather solutions with the second harmonics close to the upper edge of the phonon band. Delocalization of the second harmonics near the upper edge of 1:2 resonance region gives rise to phonon-breather solutions obtained in that resonance region.

Both in-phase and out-of-phase two-site discrete breather solutions are found to have no symmetry and to be unstable for all the frequencies the breathers exist. The region of in-phase breathers existence coincides with the region of existence of single-site breather solutions, while out-of-phase breathers could be continued up to the coupling $C=1$ (our realistic system) only for frequencies close to 1:2 resonance region.

The single-well discrete breather solutions with the second harmonics below the phonon band have not been obtained in this study because of the numerical failure of the Newton method. Some modification of computational technique is required to consider low-frequency periodic solutions with the trajectories of central particles close to the top of the interwell potential barrier. A detailed study of discrete breather solutions with two-well central particle oscillations, which can be compared to the results for the Klein-Gordon chain with double-well on-site potential [41,42], as well as of multiwell rotobreather solutions, would be a promising topics for future investigations.

As a final remark, we have to note that all the results of existence and stability properties of one- and two-site discrete breathers reported in the present paper have been obtained using the specific parameter values of ice. For the

materials with other parameter values (our model is sensible to zig-zag angle 2α, reduced covalent bond length ρ, and reduced on-site dipole rotation barrier height $4\pi\epsilon_0 R U_B^{(0)}/q^2$) the linear phonon spectrum may admit no discrete breather solutions with the frequencies below the band, or the stability properties of some discrete breather solutions may be reversed.

ACKNOWLEDGMENTS

We thank A. V. Zolotaryuk for valuable discussions and suggestions. This work has been supported in parts by the Research Commission, University of Patras, Grant C. Caratheodory No. 1911/98, and by the INTAS Foundation under Grant INTAS 97-0368.

[1] A.A. Ovchinnikov, Zh. Eksp. Teor. Fiz. **57**, 263 (1967) [Sov. Phys. JETP **30**, 147 (1970)].
[2] A.J. Sievers and S. Takeno, Phys. Rev. Lett. **61**, 970 (1988).
[3] S. Takeno and A.J. Sievers, Solid State Commun. **67**, 1023 (1988).
[4] S. Flach and C.R. Willis, Phys. Rep. **295**, 181 (1998).
[5] R.S. MacKay and S. Aubry, Nonlinearity **7**, 1623 (1994).
[6] S. Aubry, Physica D **103**, 201 (1997).
[7] J.L. Marín and S. Aubry, Nonlinearity **9**, 1501 (1996).
[8] H.S. Eisenberg, Y. Silberberg, R. Morandotti, A.R. Boyd, and J.S. Aitchison, Phys. Rev. Lett. **81**, 3383 (1998).
[9] R. Morandotti, U. Peschel, J.S. Aitchison, H.S. Eisenberg, and Y. Silberberg, Phys. Rev. Lett. **83**, 2726 (1999).
[10] B.I. Swanson, J.A. Brozik, S.P. Love, G.F. Strouse, A.P. Shreve, A.R. Bishop, W.-Z. Wang, and M.I. Salkola, Phys. Rev. Lett. **82**, 3288 (1999).
[11] U.T. Schwarz, L.Q. English, and A.J. Sievers, Phys. Rev. Lett. **83**, 223 (1999).
[12] E. Trias, J.J. Mazo, and T.P. Orlando, Phys. Rev. Lett. **84**, 741 (2000).
[13] P. Binder, D. Abraimov, A.V. Ustinov, S. Flach, and Y. Zolotaryuk, Phys. Rev. Lett. **84**, 745 (2000).
[14] A. Xie, L. van der Meer, W. Hoff, and R.H. Austin, Phys. Rev. Lett. **84**, 5435 (2000).
[15] J.F. Nagle and S. Tristam-Nagle, J. Membr. Biol. **74**, 1 (1983).
[16] G.A. Jeffrey, *An Introduction to Hydrogen Bonding* (Oxford University Press, New York, 1997).
[17] V.Ya. Antonchenko, A.S. Davydov, and A.V. Zolotariuk, Phys. Status Solidi B **115**, 631 (1983).
[18] A.V. Zolotariuk, K.H. Spatschek, and E.W. Laedke, Phys. Lett. **101A**, 517 (1984).
[19] J. Halding and P.S. Lomdahl, Phys. Rev. A **37**, 2608 (1988).
[20] J.Z. Xu and J.N. Huang, Phys. Lett. A **197**, 127 (1995).
[21] G. Kalosakas, A.V. Zolotaryuk, G.P. Tsironis, and E.N. Economou, Phys. Rev. E **56**, 1088 (1997).
[22] E.S. Kryachko and V.P. Sokhan, in *Proton Transfer in Hydrogen-Bonded Systems*, edited by T. Bountis (Plenum Press, New York, 1992), p. 105.
[23] A.V. Savin and Y. Zolotaryuk, Phys. Lett. A **201**, 213 (1995).
[24] B. Zhou and J.Z. Xu, Chaos, Solitons Fractals **9**, 429 (1997).
[25] A.V. Zolotaryuk and St. Pnevmatikos, Phys. Lett. A **143**, 233 (1990).
[26] S. Pnevmatikos, A.V. Savin, A.V. Zolotaryuk, Yu.S. Kivshar, and M.J. Velgakis, Phys. Rev. A **43**, 5518 (1991); S. Pnevmatikos, Yu.S. Kivshar, M.J. Velgakis, and A.V. Zolotaryuk, Phys. Lett. A **173**, 43 (1993).
[27] A. Zolotaryuk and St. Pnevmatikos, in *Proceedings of the International Conference on Singular Behaviour and Nonlinear Physics*, edited by St. Pnevmatikos, T. Bountis, and Sp. Pnevmatikos (World Scientific, Singapore, 1988), Vol. 2, p. 384.
[28] B. Zhou and J.Z. Xu, Phys. Lett. A **236**, 322 (1997).
[29] A.V. Zolotaryuk, P. Maniadis, and G.P. Tsironis, Physica B **296**, 251 (2001).
[30] Y.S. Kivshar and N. Flytzanis, Phys. Rev. A **46**, 7972 (1992).
[31] M. Aoki, S. Takeno, and A.J. Sievers, J. Phys. Soc. Jpn. **62**, 4295 (1993).
[32] O.A. Chubykalo and Y.S. Kivshar, Phys. Rev. E **48**, 4128 (1993); **49**, 5906 (1994).
[33] S.A. Kiselev, S.R. Bickham, and A.J. Sievers, Phys. Rev. B **48**, 13 508 (1993); **50**, 9135 (1994).
[34] T. Cretegny, R. Livi, and M. Spicci, Physica D **119**, 88 (1998).
[35] G. Huang and B. Hu, Phys. Rev. B **57**, 5746 (1998).
[36] N. Flytzanis, B.A. Malomed, and A. Neuper, Physica D **113**, 191 (1998).
[37] A.S. Kovalev, O.V. Usatenko, and A.V. Gorbatch, Phys. Rev. E **60**, 2309 (1999).
[38] M. Hörnquist, E. Lennholm, and C. Basu, Physica D **136**, 93 (2000).
[39] J.L. Marín, S. Aubry, and L.M. Floria, Physica D **113**, 283 (1998).
[40] J.L. Marín and S. Aubry, Physica D **119**, 163 (1998).
[41] S. Neusüss and R. Schilling, Phys. Rev. E **60**, 6128 (1999).
[42] E. Coquet, M. Remoissenet, and P. TchofoDinda, Phys. Rev. E **62**, 5767 (2000).
[43] P. Maniadis, A.V. Zolotaryuk, and G.P. Tsironis (unpublished).
[44] T. Cretegny, S. Aubry, and S. Flach, Physica D **119**, 73 (1998).
[45] Referring to the geometry in Fig. 1, there is no difference between the breathers with excited $(n-1,n)$ or $(n,n+1)$ sites because of the system symmetry. Upon a turn of our two-dimensional chain upside down we get the same system, but a local geometry of a pair $(n-1,n)$ turns into $(n,n+1)$ geometry.